10.1098/rsta.2003.1348

THE ROYAL SOCIETY

Tip-enhanced optical spectroscopy

By Achim Hartschuh, Michael R. Beversluis, Alexandre Bouhelier and Lukas Novotny

The Institute of Optics, University of Rochester, Rochester, NY 14627, USA (hartschuh@chemie.uni-siegen.de)

Published online 13 February 2004

Spectroscopic methods with high spatial resolution are essential for understanding the physical and chemical properties of nanoscale materials including biological proteins, quantum structures and nanocomposite materials. In this paper, we describe microscopic techniques which rely on the enhanced electric field near a sharp, laser-irradiated metal tip. This confined light-source can be used for the excitation of various optical interactions such as two-photon excited fluorescence or Raman scattering. We study the properties of the enhanced fields and demonstrate fluorescence and Raman imaging with sub-20 nm resolution.

Keywords: near-field optics; Raman spectroscopy; fluorescence imaging; second-harmonic generation

1. Introduction

The general aim of near-field optical microscopy is to extend spatial optical resolution beyond the diffraction limit (Lewis *et al.* 1984; Pohl *et al.* 1984). The introduction of the aperture probe (Betzig & Trautman 1992) for near-field microscopy has allowed fluorescence imaging with sub-diffraction resolution and has stimulated interests in many disciplines, especially the material and biological sciences (see, for example, Dunn 1999). The widely adopted aperture approach is based on an aluminium-coated fibre tip of which the foremost end is left uncoated to form a small aperture. Unfortunately, only a tiny fraction (up to 10^{-4} for a 100 nm aperture) of the light coupled into the fibre is emitted by the aperture because of the cut-off of propagating waveguide modes (Novotny & Pohl 1995).

The use of laser-illuminated metal tips for near-field imaging has been discussed by many groups. In general, two different types can be distinguished.

Scattering-type microscopy. Here the tip locally perturbs the fields near a sample surface (see, for example, Knoll & Keilmann 1999). The response to this perturbation is detected in the far-field at the same frequency of the incident light only, and contains both near-field and far-field contributions.

Tip-enhanced microscopy (Wessel 1985). Locally enhanced fields at laser illuminated metal structures are used to increase the spectroscopic response of the system studied within a small sample volume (e.g. Hartschuh *et al.* 2003; Hayazawa

One contribution of 13 to a Theme 'Nano-optics and near-field microscopy'.

 © 2004 The Royal Society

et al. 2001; Sánchez *et al.* 1999; Stöckle *et al.* 2000). The flexibility of the technique allows the study of a variety of spectroscopic signals, including local fluorescence or Raman spectra, as well as time-resolved measurements such as fluorescence transients.

Section 2 contains a brief theoretical description of electric field enhancement at a metal tip. Using this information, the experimental requirements and expected properties of the fields are discussed. In the § 3, the general experimental set-up is introduced. In the following three sections, applications of tip-enhanced spectroscopy are demonstrated: second-harmonic generation, two-photon excited fluorescence and Raman scattering.

2. Field-enhancement at a metal tip

Field enhancement near nanoscale metal structures plays a central role in optical phenomena such as surface-enhanced Raman scattering (SERS), second-harmonic (SH) generation and near-field microscopy. The enhancement originates from a combination of the electrostatic lightning-rod effect, which is due to the geometric singularity of sharply pointed structures, and localized surface plasmon resonances which depend sensitively on the excitation wavelength. The incident light drives the free electrons in the metal along the direction of polarization. While the charge density is zero inside the metal at any instant of time, charges accumulate on the surface of the metal. When the incident polarization is perpendicular to the tip axis, diametrically opposed points on the tip surface have opposite charges. As a consequence, the foremost end of the tip remains uncharged and no field enhancement is achieved. On the other hand, when the incident polarization is parallel to the tip axis, the induced surface charge density is almost rotationally symmetric and has the highest amplitude at the end of the tip (Larsen & Metiu 2001; Martin *et al.* 2001; Novotny *et al.* 1998).

The calculated field distribution $[|E_{\mathrm{local}}(\boldsymbol{r},\omega)|^2]$ within a plane parallel to the tip axis near a sharp gold tip located above a glass substrate and irradiated by an on-axis focused Hermite Gaussian (1,0) laser mode is presented in figure 1*a*. The figure demonstrates that the enhanced field is confined to the tip apex (diameter 20 nm) in all three dimensions. The illuminated tip thus represents a nanoscale light source. The maximum enhancement of the electric field intensity $M = |E_{\mathrm{local}}(\boldsymbol{r},\omega)|^2/|E_{\mathrm{in}}(\boldsymbol{r},\omega)|^2$ calculated for a solid gold tip with a diameter of 10 nm at an excitation wavelength of 830 nm is around 250.

To establish a strong field enhancement at the tip, the electric field of the exciting laser beam needs to be polarized along the tip axis. The influence of tip shape and material on the field enhancement has been discussed in a series of publications with the aim to find the optimum tip (Krug *et al.* 2002; Martin *et al.* 2001).

3. Experimental set-up

The experimental set-up is based on an inverted optical microscope with an x, y scan stage for raster scanning a transparent sample. The light source for SH and two-photon excitation is a mode-locked Ti-sapphire laser providing 100 fs pulses tunable between 720 and 960 nm. For Raman experiments a continuous-wave laser at 633 nm

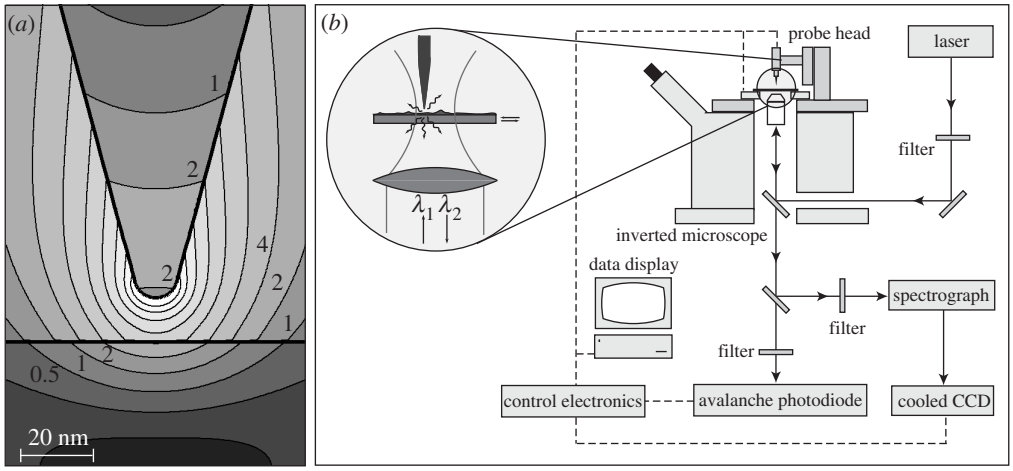

Figure 1. (*a*) Calculated field distribution $[|E_{\mathrm{local}}(\boldsymbol{r},\omega)|^2]$ near a gold tip located above a glass substrate and irradiated by an on-axis focused Hermite Gaussian (1,0) laser mode. The contour lines scale by a factor of two. (*b*) Schematic of the experimental set-up. A sharp metal tip is scanned through a tightly focused laser beam. The optical signal is detected either by an APD or by a combination of spectrograph and a CCD.

is used. The laser beam is reflected by a dichroic beam splitter and focused by a high-numerical-aperture (high-NA) objective (1.4 NA) on the sample surface. A sharp gold or silver tip is positioned near the focus of the beam and maintained above the sample surface at a distance of *ca.* 1–2 nm by means of a sensitive shear-force feedback mechanism (Karrai & Grober 1995). The optical signal is collected with the same objective, transmitted by the beam splitter and filtered by a long or bandpass filter to remove the fundamental laser light. The signal is detected either by a combination of a spectrograph and a cooled charge-coupled device (CCD) or by a narrow bandpass filter followed by a single-photon counting avalanche photodiode (APD). A near-field optical image is established by raster scanning the sample and simultaneously recording the optical signal. Sharp gold and silver tips are produced by electrochemical etching followed by focused ion beam milling (FIB) in the case of silver. SEM images of the tips are taken before and after scanning to ensure well-defined tip shapes.

To establish a strong field enhancement at the tip, the electric field of the exciting laser beam needs to be polarized along the tip axis (see § 2). To achieve this condition in our on-axis illumination scheme, we displace the tip from the centre of the beam in the direction of polarization into one of the two longitudinal field lobes characteristic for strongly focused Gaussian beams or we use higher-order laser modes such as the Hermite Gaussian (1,0) mode or the radially polarized mode (Novotny *et al.* 1998; Quabis *et al.* 2000) with strong longitudinal fields in the centre of the focus.

4. Second-harmonic generation

Second-harmonic generation (SHG) in gold has been studied extensively in the context of near-field optical microscopy (Bozhevolnyi & Lozovski 2002; Novotny *et al.* 1998; Smolyaninov *et al.* 2001; Zayats *et al.* 2000). In most of these investigations,

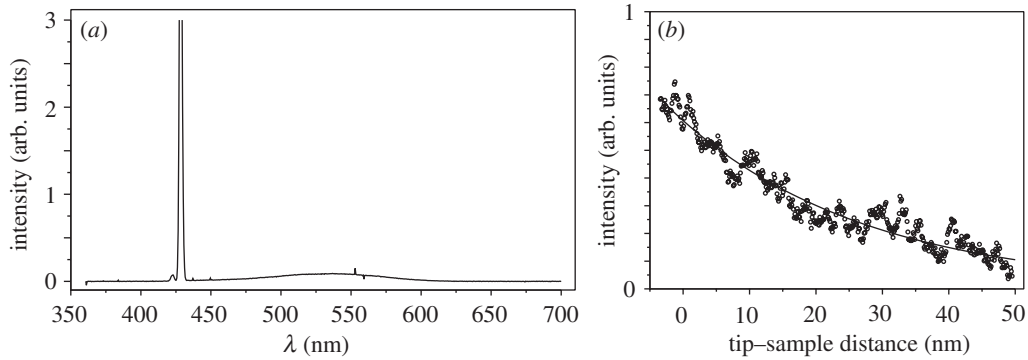

Figure 2. (*a*) Spectrum detected for a gold tip after fs-pulse excitation at 860 nm by the longitudinal field of a tightly focused Gaussian laser beam. A huge second-harmonic peak at 430 nm and a weak broadband continuum are observed. (*b*) Evolution of the second-harmonic intensity as a function of tip–sample separation (circles). The solid line represents an exponential fit with a decay length of 25 nm.

thin metallic films were excited by a femtosecond laser pulse coupled to a near-field optical probe. These studies revealed that the generation of the SH light is not distributed homogeneously over the film surface but arises mainly from randomly located confined regions (Bozhevolnyi *et al.* 2003). The increased SH responses of these regions were found to correlate with large electromagnetic field enhancement mainly originating from local excitation of resonant surface plasmons.

In this section, the direct connection between field enhancement and SHG is demonstrated experimentally using sharp gold tips with well-defined sizes and shapes. Furthermore, the observed SH intensity can be used to quantify the field enhancement achieved in the experiment. We show that the generation of SH light is confined to the tip apex and discuss the applicability of the tip-controlled SHG as a nanoscale light source.

In our experiment, a sharp gold tip is placed in the focal region of a diffraction-limited femtosecond laser beam with a wavelength of 860 nm (see figure 1*b*). The tip is positioned into one of the two longitudinal field lobes of a focused Gaussian beam to maximize the expected field enhancement effect (Bouhelier *et al.* 2003*b*). Figure 2*a* shows a typical emission spectrum of a gold tip. The spectrum is dominated by a sharp peak at 430 nm (twice the excitation frequency) caused by SHG at the tip. Additionally, a weak, broadband emission continuum is observed which is discussed elsewhere (Beversluis *et al.* 2003).

As discussed in § 2, a strong field enhancement is established only for light polarized parallel to the tip axis (longitudinal fields). Since efficient SHG requires field enhancement, the SH intensity should also be sensitive to this field polarization. Figure 3*a* shows the intensity of the SH signal emitted by a gold tip which is raster scanned through the focal spot of a Gaussian laser beam. The highest intensities are located in two equally bright spots oriented parallel to the incident polarization direction (vertical in the figure). Figure 3*b* represents the calculated longitudinal field distribution in a focused Gaussian beam using the experimental parameters. Here too, the intensity is confined in a two-lobe region. The similarity between figure 3*a* and figure 3*b* indicates that the SH signal is generated only when the tip is excited by fields polarized along its axis. To further confirm this result, the same gold tip

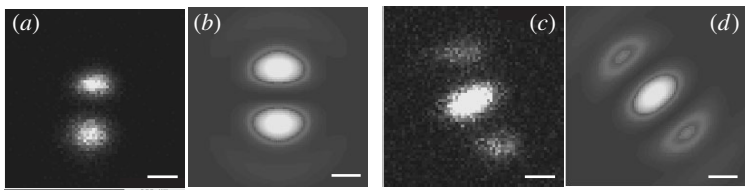

Figure 3. The intensity of the SH signal emitted by a gold tip which is raster scanned through the focus of (*a*) a Gaussian and (*c*) a Hermitian–Gaussian beam, respectively. Calculated distributions of the longitudinal fields in the focus of (*b*) a Gaussian and (*d*) a Hermitian–Gaussian beam, respectively. The scale bar is 250 nm.

was raster scanned through the focal region of a Hermitian–Gaussian $(1,0)$ beam $[HG_{10}]$. Figure 3*c*, *d* shows the SH distribution and the calculated longitudinal field component, respectively. The agreement between the two images confirms the direct correlation between SHG and longitudinal field polarization. Field enhancement and SHG are therefore sensitive to the same excitation conditions.

The SH images in figure 3*a*, *c* produced by the tip emission correspond to the characteristic fluorescence images rendered by a single molecule having a transition dipole moment oriented in longitudinal direction (parallel to the tip) (Sick *et al.* 2000). Based on this analogy, a theoretical model for the excitation and emission of SH radiation at the tip has been developed (Bouhelier *et al.* 2003*a*). It was found that the SH response can be modelled by a single dipole located in the centre of the tip apex and oriented along the main axis of the tip. As a consequence, the field distribution of the SH signal generated by the tip can be represented by the field distribution of this dipole. The strength of the dipole is directly proportional to the field enhancement factor allowing for a quantification of the enhancement achieved.

We observed variations of the SH signal from tip to tip. Electro-chemically etched gold tips have a broad distribution of cone angles, apex diameters, or degrees of symmetry. The sensitivity of the second-harmonic generation to these variations indicates a direct relation between the enhancement capability of a tip and its nonlinear response and can help in finding the geometry that can render the strongest enhancement.

The near-field nature of second-harmonic generation is revealed in figure 2*b*. The graph (circles) shows a monotonous increase of the SH intensity as the tip approaches the surface. The solid line represents a single exponential fit to the data. The decay length is 25 nm, a value of the order of the tip size. Second-harmonic generation is therefore localized to the very end of the tip.

The availability of a confined and tunable second-harmonic light source opens the possibility of nanoscale absorption spectroscopy on length-scales comparable to the tip's size. However, preliminary studies on semiconductor nanoparticles and metalloproteins indicate that the contrast mechanism of recorded optical transmission images is not only of spectroscopic origin but mostly dominated by scattering at topographic features. As the tip moves over a feature, the SH intensity is reduced because the tip is pulled out from the region of highest longitudinal field strength (see figure 2*b*). As a result, the transmitted signal is decreased, leading to a well-known topography-induced artefact (Hecht *et al.* 1997). In order to have true spectroscopic contrast, the sample under investigation needs to have a flat surface (arranged in monolayers or embedded in a polymer matrix).

5. Two-photon excited fluorescence

Fluorescence microscopy is a valuable technique used extensively in biology and medical research. However, the length-scale of many biological systems of interest, such as single proteins, is of the order of 10 nm. This is far below the diffraction limit for visible wavelengths, and even beyond the reach of aperture-type near-field optical microscopes. Because the spatial resolution of tip-enhanced techniques is limited only by the tip size, optical spectroscopy of single proteins seems to be achievable.

A key issue in near-field fluorescence imaging with metal tips is the rejection of the far-field background signal from the entire illuminated area. In order to enhance the near-field contrast, we use two-photon excitation of fluorescence. Since two-photon excitation is a nonlinear process with quadratic dependence on excitation intensity, the detected fluorescence signal becomes proportional to the square of the intensity enhancement factor M^2 (Sánchez *et al.* 1999).

The flux of fluorescence photons Φ_{fl} upon laser illumination at frequency ω_{I} and intensity I_{I} can be calculated using the two-photon absorption cross-section of the sample $\sigma_{2\mathrm{ph}}(\omega_{\mathrm{I}})$ and the fluorescence quantum yield of the emitter in the presence of the tip Q_{fl}:

$$\Phi_{\mathrm{fl}} = \frac{I_{\mathrm{I}}^2}{\hbar^2\omega_{\mathrm{I}}^2}\sigma_{2\mathrm{ph}}Q_{\mathrm{fl}}M^2. \tag{5.1}$$

The high peak intensities required for a multi-photon process can be provided by ultrafast laser systems with pulse widths in the range of hundreds of femtoseconds (full width, half-maximum, FWHM). Higher-order excitation processes are possible too, however, photodamage of the sample at high excitation densities has to be considered.

Near-field fluorescence imaging with 20 nm resolution of two different materials was first reported by (Sánchez *et al.* 1999) and our group continued the study of J-aggregates of pseudoisocyanine (PIC) dye. Figure 4 shows the simultaneously recorded near-field image and the topographic shear-force image of PIC J-aggregates embedded in a polyvinyl siloxane (PVS) film. The optical image is formed by collecting the fluorescence signal after non-resonant excitation at 830 nm using an appropriate bandpass filter (transmission between 550 and 750 nm) followed by an APD. In both images, characteristic one-dimensional strands of J-aggregates are observed, confirming a close correlation between topographic and optical image. The cross-section shown in figure 4*d* features a width of *ca.* 25 nm, demonstrating clear sub-diffraction resolution.

While the two images in figure 4 are similar, it has to be emphasized that the optical image contains far more information than the topographic image. By selecting multiple spectral detection ranges, different emitting species with different fluorescence spectra can be imaged simultaneously, offering a wealth of spectroscopic information.

More precisely, the image formed by fluorescence microscopy not only shows the fluorescence properties but a combination of both two-photon absorption cross-section and fluorescence properties of the sample. In fact, because of the fast energy transfer in J-aggregates, the detected signal can originate from a location displaced from the position of excitation.

Furthermore, the pulsed excitation of the sample offers the possibility for time-resolved fluorescence measurements. Using time-correlated single photon counting

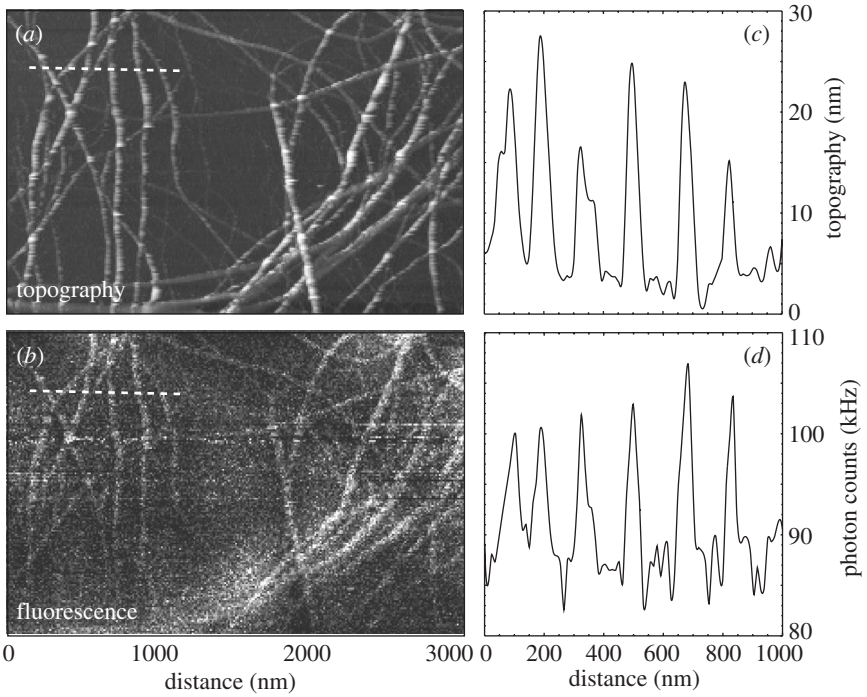

Figure 4. Simultaneous (*a*) topographic image and (*b*) near-field two-photon excited fluorescence image of J-aggregates of PIC dye in a PVS film on a glass substrate. Cross-sections along the dashed white lines indicate that the optical image (*d*) has slightly better resolution than the topographic image (*c*) (FWHM of 25 nm against 30 nm).

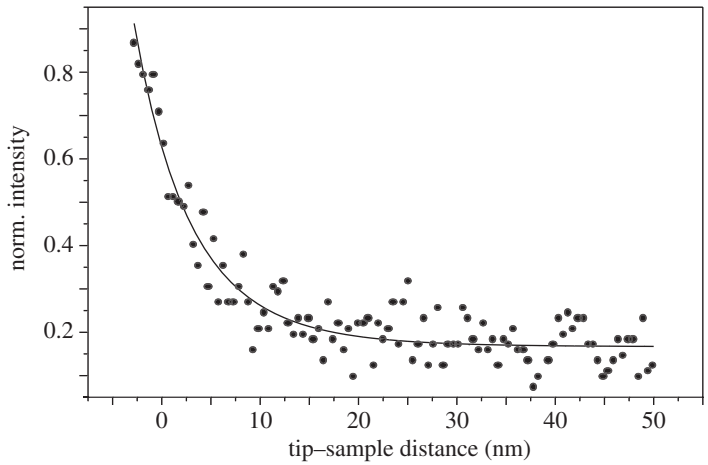

Figure 5. Distance dependence of the two-photon excited fluorescence from J-aggregates after femtosecond excitation at 833 nm.

(TCSPC), the combination of near-field optics and ultrafast spectroscopy is readily achieved. The observation of photo-induced processes, such as charge transfer, energy transfer or isomerization reactions on the nanoscale is feasible.

The optical resolution apparent in figure 4 shows that the enhanced field is laterally confined to the size of the metal tip. To demonstrate the confinement of the enhanced fields in the longitudinal direction, the tip is positioned above a J-aggregate and the fluorescence intensity is recorded as a function of tip–sample distance, d. According to equation (5.1), the signal strength is expected to scale with the fourth power of the enhanced field. The latter can be approximated well by the field of a single dipole oriented along the tip axis and thus in the near-field it can be expected that the experimental signal scales with d^{-12}, with d being the distance between dipole origin and sample surface. This dependence is verified in our experiments if one takes into account that the tip–sample distance equals $(d-r_0)$, with r_0 being the tip radius (figure 5).

Because of the small separation between emitter and metal tip (*ca.* 1–2 nm), non-radiative energy transfer from the electronically excited molecule to the metal has to be taken into account. This process would represent an additional relaxation pathway and would reduce the number of detected fluorescence photons. While the theory of energy transfer between molecules and flat metal interfaces is well understood in the framework of phenomenological classical theory (Barnes 1998; Chance *et al.* 1978), nanometre-sized objects are more difficult to describe than flat interfaces. For extended silver interfaces, the lifetime of a molecule on top of the interface is reduced by more than two orders of magnitude compared with the lifetime in free space. For a sharp metal tip, the quenching effect can be expected to be smaller because the interaction area is reduced. Furthermore, although the excited-state lifetime of a molecule is reduced close to metal nanostructures, the balance between radiative and non-radiative decay rates depends sensitively on the particular geometry. The measured distance dependence shown in figure 5 follows the expected d^{-12} dependence and gives no indication of a strong quenching effect. Of course, quenching of J-aggregates is strongly reduced because of the fast excitonic delocalization of the excitation energy (Sánchez *et al.* 1999).

6. Raman scattering

Fluorescence imaging requires a high-fluorescence quantum yield of the system studied or artificial labelling with fluorophores. Furthermore, fluorescence spectra of organic molecules are often broad and featureless, impeding their clear identification within complex systems. On the other hand, Raman scattering probes the unique vibrational spectrum of the sample and reflects its chemical composition and molecular structure directly. The main drawback of Raman scattering is the extremely low scattering cross-section, which is typically 14 orders of magnitude smaller than the cross-section of fluorescence. SERS, induced by nanometre-sized metal structures, has been shown to provide enormous enhancement factors of up to 10^{15}, allowing for Raman spectroscopy even on the single-molecule level (see, for example, Nie & Emory 1997). The strongest contribution to SERS is of electromagnetic origin, caused by the enhancement of the local field E^{L} with respect to the incident field E^{I}. For the present studies, we do not expect significant contributions from chemical effects based on charge-transfer processes between scatterer and metal or overlapping electron wave functions due to the large tip–sample separation of more than 1 nm.

The electromagnetic enhancement factor M_i is defined as the ratio between the measured Raman cross-section in the presence and in the absence of the metal surface

for each scatterer i. The integrated photon flux Φ_{Raman} is a linear function of the intensity of the incident laser light I_{I} at frequency ω_{I} and results from the sum of the Raman scattering cross-sections σ_i^{R} of all scatterers within the detection volume:

$$\Phi_{\mathrm{Raman}} = \frac{I_{\mathrm{I}}}{\hbar\omega_{\mathrm{I}}} \sum_{i=1}^{N} \sigma_i^{\mathrm{R}} M_i. \tag{6.1}$$

The electromagnetic enhancement M_i is caused by enhancement of both the incident field E^{I} at ω_{I} and the scattered field E^{I} at $\omega_{\mathrm{I}} - \omega_\nu$, where ω_ν is the vibrational frequency, and can be expressed as the product with the total local electric field E^{L},

$$M_i = \left[\frac{E^{\mathrm{L}}(\omega_{\mathrm{I}})}{E^{\mathrm{I}}(\omega_{\mathrm{I}})}\right]^2 \left[\frac{E^{\mathrm{L}}(\omega_{\mathrm{I}} - \omega_\nu)}{E^{\mathrm{I}}(\omega_{\mathrm{I}} - \omega_\nu)}\right]^2 \approx \left[\frac{E^{\mathrm{L}}(\omega_{\mathrm{I}})}{E^{\mathrm{I}}(\omega_{\mathrm{I}})}\right]^4, \tag{6.2}$$

where we used $\omega_\nu \ll \omega_{\mathrm{I}}$.

Enhancement factors reaching up to 12 orders of magnitude are reported for particular multiple-particle configurations involving interstitial sites between particles or outside sharp surface protrusions (Xu *et al.* 2000). For a single spherical particle, M is supposed to be much lower, in the range 100–1000. Near-field Raman scattering induced by a laser-irradiated metal tip has been experimentally demonstrated in Stöckle *et al.* (2000), Nieman *et al.* (2001), Hayazawa *et al.* (2002) and Hartschuh *et al.* (2003). In this section, we present near-field Raman imaging and spectroscopy on single-walled carbon nanotubes (SWNTs). The three major advantages of the method are demonstrated: high spatial resolution, signal enhancement (enhanced sensitivity) and chemical specificity.

SWNTs are highly elongated tubular graphitic molecules, which have been the focus of intense interest due to a large variety of potential technological applications. The unique properties of SWNTs arise from their particular one-dimensional structure, which is directly linked to the characteristic Raman bands. Raman scattering of SWNTs has been studied intensively in the literature (see, for example, Duesberg *et al.* 2000; Jorio *et al.* 2001) and Raman enhancements of up to 10^{12} have been reported for tubes in contact with fractal silver colloidal clusters (Kneipp *et al.* 2000).

In figure 6*a* a near-field Raman image of SWNTs on glass is shown together with the simultaneously acquired topography image of the same sample area in figure 6*b*. Raman images were acquired by detecting the intensity of the G band around 1600 cm^{-1} after laser excitation at 633 nm using a radially polarized laser mode while raster scanning the sample. The spatial resolution can be determined from the width of the signals presented as line scans in figure 6*c*, *d* to be *ca.* 20 nm. The sharpest images observed so far feature an optical resolution of *ca.* 12 nm, limited by the tip diameter. The height of the observed SWNT is *ca.* 1 nm, as can be seen in figure 6*d*.

Raman spectra detected on top of an SWNT in the presence of the tip and without tip is presented in figure 7*a*. The signal enhancement induced by the tip can be estimated by comparison of the integrated intensities of the observed Raman band. In the present example, the intensity of the G band of the SWNT between 1500 and 1650 cm^{-1} is approximately 12000 (background subtracted). In absence of the tip, the signal is much weaker (up to 100). From figure 7*a* it is clear that, without

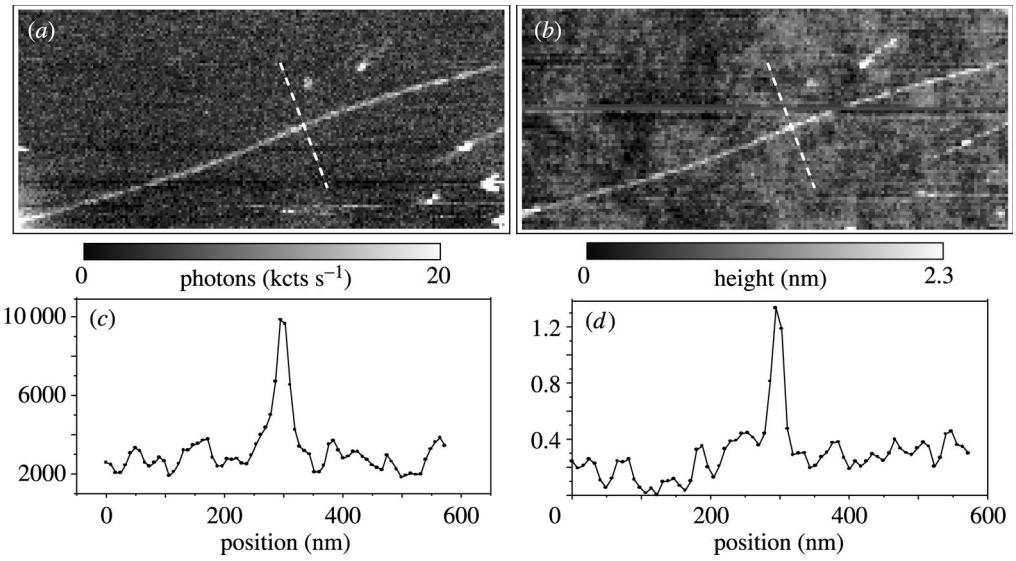

Figure 6. Simultaneous (*a*) near-field Raman image and (*b*) topographic image of SWNTs on glass. Scan area, $2 \times 1\ \mu m^2$. The Raman image is acquired by detecting the intensity of the G band upon laser excitation at 633 nm. The dark regions in the topography image are caused steps within the glass. (*c*) Cross-section taken along the indicated dashed line in the Raman image. (*d*) Cross-section taken along the indicated dashed line in the topographic image. The height of the individual tube is *ca.* 1.0 nm. Vertical units are photon counts per second for (*c*) and nanometres for (*d*).

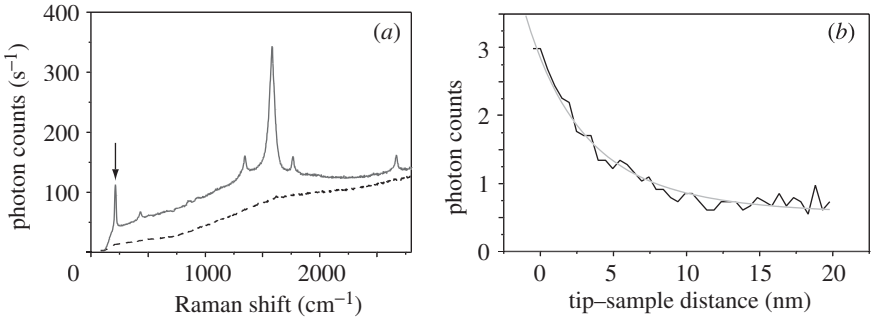

Figure 7. Tip-enhanced Raman spectra of SWNTs. (*a*) Spectra detected with tip on top of an SWNT (solid line) and with tip retracted by 2 μm (dashed line). The Raman signal of the radial breathing mode (RBM) is marked. Both spectra are on top of a broad background which is caused by scattering from cover glass and the immersion oil (also detected in the absence of SWNTs). (*b*) Dependence of the Raman scattering strength of the G band on the longitudinal separation between a single SWNT and the tip for small distances of less than 20 nm. The grey line is a model curve using a d^{-12} dependency.

the enhancement provided by the tip, the detection of the SWNT would have been impossible.

For an evaluation of the enhancement factor, the different areas probed by near-field and far-field components must be taken into account. The length of the SWNT (width $w \approx 1$ nm) is larger than the diameter of the focus ($f = 300$ nm), resulting

in a probed area of approximately $fw = 1\,\mathrm{nm} \times 300\,\mathrm{nm} = 300\,\mathrm{nm}^2$. A much smaller area is probed in the near-field, i.e. an area defined by the width of the near-field spot (15 nm) and the tube diameter (*ca.* 1 nm). Normalizing the measured signals in figure 7*a* with the ratio of the detected areas yields an enhancement factor of $M \approx 2400$. Since M scales approximately with the fourth power of the field enhancement, the locally enhanced field is roughly seven times stronger than the incident field.

Potential modifications of the Raman lines or changes in their relative amplitudes caused by the tip have not been observed so far, but would be difficult to distinguish. Far-field spectra arise from a superposition of all Raman signals within the confocal detection volume whereas near-field spectra are sensitive to local variations, such as structural defects. Any comparison between near-field and far-field spectra has to distinguish between possible modifications caused by the tip and local fluctuations of the Raman signals caused by structural variations.

The chemical specificity of the near-field Raman method was used by (Hartschuh *et al.* 2003) to distinguish between SWNTs and humidity related water contaminations on the sample surface. This specificity can be used to detect nanotube structure and to distinguish between SWNTs of different types. The spectral position of the radial breathing mode peak in figure 7 of $\nu_{\mathrm{RBM}} = 199.0\,\mathrm{cm}^{-1}$ matches the calculated value for a metallic SWNT with structural parameters $(14, 2)$, which renders $\nu_{\mathrm{RBM}} = 198.9\,\mathrm{cm}^{-1}$ and a diameter of $d = 1.2\,\mathrm{nm}$ (Bachilo *et al.* 2002) $(d = 223.5\,\mathrm{nm}/(\nu_{\mathrm{RBM}} - 12.5\,\mathrm{cm}^{-1}))$.

According to equation (6.2), the signal strength is expected to scale with the fourth power of the enhanced field. If we approximate the enhanced field by the field of a single dipole oriented along the tip axis, a distance dependence of d^{-12} is expected as for the two-photon excitation of fluorescence in § 5. The Raman scattering strength recorded as a function of tip–sample distance d shown in figure 7 can be well described using a d^{-12} dependence (grey line in figure 7).

7. Outlook

The spatial resolution achieved in tip-enhanced near-field microscopy and spectroscopy is generally superior to aperture-based techniques. The field confinement is defined by the sharpness of the tip and the field distribution is approximated reasonably well by the field of a dipole oriented in direction of tip axis and located in the centre of the tip apex. It is likely that the tip enhancement technique will provide resolutions better than 10 nm, a length-scale comparable to biological proteins and semiconductor quantum structures. To become a routine technique, the field enhancement needs to be improved using favourable tip materials and geometries. In analogy to antenna theory, a finite tip size (e.g. $\lambda/2$) is expected to provide much higher enhancement. It is also desirable to reduce the far-field interaction area with the sample surface and to combine, for example, an aperture near-field probe with a finite-sized metal tip (Frey *et al.* 2003). To clarify the trade-off between enhancement and quenching, dedicated experiments on single molecules are necessary. These studies require the simultaneous measurements of fluorescence yield and lifetime, and the investigation of orientational and polarization properties (Novotny 1996). Applied to Raman scattering, the tip-enhancement technique has great potential for clarifying open questions in SERS.

The authors acknowledge stimulating discussions with Todd D. Krauss, Neil Anderson, X. Sunney Xie and Erik J. Sànchez. This work was funded by the US Department of Energy (grant DE-FG02-01ER15204), the National Science Foundation (grants DMR-0078939 and BES-0086368), and partly by the Swiss National Science Foundation through a postdoctoral fellowship to A.B.

References

Bachilo, S. M., Strano, M. S., Kittrell, C., Hauge, R. H., Smalley, R. E. & Weisman, R. B. 2002 Structure-assigned optical spectra of single-walled carbon nanotubes. *Science* **298**, 2361–2366.

Barnes, W. L. 1998 Fluorescence near interfaces: the role of photonic mode density. *J. Mod. Opt.* **45**, 661–669.

Betzig, E. & Trautman, J. K. 1992 Near-field optics: microscopy, spectroscopy, and surface modification beyond the diffraction limit. *Science* **257**, 189–195.

Beversluis, M. R., Bouhelier, A. & Novotny, L. 2003 Continuum generation from single gold nanostructures through near-field mediated intraband transitions. *Phys. Rev.* B **68**, 115433.

Bouhelier, A., Beversluis, M., Hartschuh, A. & Novotny, L. 2003*a* Near-field second-harmonic generation induced by local field enhancement. *Phys. Rev. Lett.* **90**, 013903.

Bouhelier, A., Beversluis, M. R. & Novotny, L. 2003*b* Near-field scattering of longitudinal fields. *Appl. Phys. Lett.* **82**, 4596–4598.

Bozhevolnyi, S. I. & Lozovski, V. Z. 2002 Second-harmonic scanning optical microscopy of individual nanostructures. *Phys. Rev.* B **65**, 235420.

Bozhevolnyi, S. I., Beerman, J. & Coello, V. 2003 Direct observation of localized second-harmonic enhancement in random metal nanostructures. *Phys. Rev. Lett.* **90**, 197403.

Chance, R. R., Prock, A. & Silbey, R. 1978 Molecular fluorescence and energy transfer near interfaces. In *Advances in chemical physics* (ed. I. Progogine & S. A. Rice), vol. 37, pp. 1–65. Wiley.

Duesberg, G. S., Loa, I., Burghard, M., Syassen, K. & Roth, S. 2000 Polarized Raman spectroscopy on isolated single-wall carbon nanotubes. *Phys. Rev. Lett.* **85**, 5436–5439.

Dunn, B. 1999 Near-field scanning optical microscopy. *Chem. Rev.* **99**, 2891–2928.

Frey, H. G., Keilmann, F., Kriele, A. & Guckenberger, R. 2003 Enhancing the resolution of scanning near-field optical microscopy by a metal tip grown on an aperture probe. *Appl. Phys. Lett.* **81**, 5030–5032.

Hartschuh, A., Sánchez, E. J., Sunney, X. S. & Novotny, L. 2003 High-resolution near-field Raman microscopy of single-walled carbon nanotubes. *Phys. Rev. Lett.* **90**, 095503.

Hayazawa, N., Inouye, Y., Sekkat, Z. & Kawata, S. 2001 Near-field Raman scattering enhanced by a metallized tip. *Chem. Phys. Lett.* **335**, 369–374.

Hayazawa, N., Inouye, Y., Sekkat, Z. & Kawata, S. 2002 Near-field Raman imaging of organic molecules by an apertureless metallic probe scanning optical microscope. *J. Chem. Phys.* **117**, 1296–1301.

Hecht, B., Bielefelt, H., Inouye, Y., Pohl, D. W. & Novotny, L. 1997 Facts and artifacts in near-field optical microscopy. *J. Appl. Phys.* **81**, 2492–2498.

Jorio, A., Saito, R., Hafner, J. H., Lieber, C. M., Hunter, M., McClure, T., Dresselhaus, G. & Dresselhaus, M. S. 2001 Structural (n, m) determination of isolated single-wall carbon nanotubes by resonant Raman scattering. *Phys. Rev. Lett.* **86**, 1118–1121.

Karrai, K. & Grober, R. D. 1995 Piezoelectric tip–sample distance control for near field optical microscopes. *Appl. Phys. Lett.* **66**, 1842–1844.

Kneipp, K. (and 10 others) 2000 Surface-enhanced and normal Stokes and anti-Stokes Raman spectroscopy of single-walled carbon nanotubes. *Phys. Rev. Lett.* **84**, 3470–3473.

Knoll, B. & Keilmann, F. 1999 Near-field probing of vibrational absorption for chemical microscopy. *Nature* **399**, 134–136.

Krug, J. T. I., Sánchez, E. J. & Xie, X. S. 2002 Design of near-field probes with optimal field enhancement by finite difference time domain electromagnetic simulation. *J. Chem. Phys.* **116**, 10 895–10 901.

Larsen, R. E. & Metiu, H. 2001 Resolution and polarization in apertureless near-field microscopy. *J. Chem. Phys.* **114**, 6851–6860.

Lewis, A., Isaacson, M., Harootunian, A. & Muray, A. 1984 Development of a 500 Å resolution light microscope. *Ultramicroscopy* **13**, 227–231.

Martin, Y. C., Hamann, H. F. & Wickramasinghe, H. K. 2001 Strength of the electric field in apertureless near-field optical microscopy. *J. Appl. Phys.* **89**, 5774–5778.

Nie, S. & Emory, S. R. 1997 Probing single molecules and single nanoparticles by surface-enhanced Raman scattering. *Science* **275**, 1102–1106.

Nieman, L. T., Krampert, G. M. & Martinez, R. E. 2001 An apertureless near-field scanning optical microscope and its application to surface-enhanced Raman spectroscopy and multiphoton fluorescence imaging. *Rev. Scient. Instrum.* **72**, 1691–1699.

Novotny, L. 1996 Single molecule fluorescence in inhomogeneous environments. *Appl. Phys. Lett.* **69**, 3806–3808.

Novotny, L. & Pohl, D. W. 1995 Light propagation in scanning near-field optical microscopy. *NATO Adv. Stud. Inst.* E **184**, 21–33.

Novotny, L., Sánchez, E. J. & Xie, X. S. 1998 Near-field optical imaging using metal tips illuminated by higher-order Hermite–Gaussian beams. *Ultramicroscopy* **71**, 21–29.

Pohl, D. W., Denk, W. & Lanz, M. 1984 Optical stethoscopy: image recording with resolution $\lambda/20$. *Appl. Phys. Lett.* **44**, 651–653.

Quabis, S., Dorn, R., Glöckl, O., Eberler, M. & Leuchs, G. 2000 Focusing light to a tighter spot. *Opt. Commun.* **179**, 1–4.

Sánchez, E. J., Novotny, L. & Xie, X. S. 1999 Near-field fluorescence microscopy based on two-photon excitation with metal tips. *Phys. Rev. Lett.* **82**, 4014–4017.

Sick, B., Hecht, B. & Novotny, L. 2000 Orientational imaging of single molecules by annular illumination. *Phys. Rev. Lett.* **85**, 4482–4485.

Smolyaninov, I. I., Liang, H. Y., Lee, C. H. & Davis, C. C. 2001 Local crystal analysis using near-field second harmonic microscopy: application to thin ferroelectric films. *J. Appl. Phys.* **89**, 206–211.

Stöckle, S. M., Suh, Y. D., Deckert, V. & Zenobi, R. 2000 Nanoscale chemical analysis by tip-enhanced Raman spectroscopy. *Chem. Phys. Lett.* **318**, 131–136.

Wessel, J. 1985 Surface enhanced optical microscopy. *J. Opt. Soc. Am.* B **2**, 1538–1540.

Xu, H., Aizpurua, J., Käll, M. & Apell, P. 2000 Electromagnetic contributions to single-molecule sensitivity in surface-enhanced Raman scattering. *Phys. Rev.* E **62**, 4318–4324.

Zayats, A. V., Kalkbrenner, T., Sandoghdar, V. & Mlynek, J. 2000 Second-harmonic generation from individual surface defects under local excitation. *Phys. Rev.* B **61**, 4545–4548.